JOURNAL DE PHYSIQUE IV
Colloque C2, supplément au Journal de Physique III, Volume 5, février 1995

γ Precipitates in Cu-Zn-Al Alloys Studied by High Resolution Electron Microscopy

J. Pons*,**(1) and R. Portier*,**

* *Lab. Métallurgie Structurale, ENSCP, 11 rue Pierre et Marie Curie, 75231 Paris cedex 05, France*
** *Centre d'Etudes de Chimie Métallurgique, CNRS , 15 rue G. Urbain, 94407 Vitry-sur-Seine, France*

Abstract. A HREM study of small γ-phase precipitates in β *Cu-Zn-Al* single crystals is presented. The images taken at atomic resolution show the perfect coherency of the precipitates when they are embedded in the β austenitic phase. In this case, the precipitates are located at the antiphase boundaries of the matrix. In turn, several microdomains separated by internal antiphase-like boundaries are present inside the precipitates. Nevertheless, the study of the boundaries at atomic level shows that the shift associated to the boundary (one atomic plane along <110>) is not a translations vector of the lattice. When the precipitates are embedded in a martensitic (18R) matrix, the precipitates loose the coherency. A mechanism of martensite/precipitate accommodation based on the formation of a small nanoplate at the interface between the main martensite plate and the precipitate, together with the formation of dislocations, has been observed.

1. INTRODUCTION

The effect of different distributions of γ-phase precipitates on the martensitic transformation in *Cu*-based shape memory alloys has been the subject of several studies reported in the last years [1-10]. In the case of *Cu-Zn-Al* single crystals, the most interesting effects have been obtained with dense distributions of small and coherent precipitates (sizes of the order of 100-200 nm). Besides the hardening of the alloys produced by the coherent precipitates [11], these precipitate distributions improve the stability of the martensitic transformation temperatures during thermal cycling (up to several hundreds of cycles) [8,9] as well as reduce one order of magnitude the number of pseudoelastic cycles needed to induce the two-way shape memory effect by pseudoelastic cyling [10].

The small precipitate size makes very difficult the observation of fine details by means of conventional TEM, being necessary the use of HREM. In this work we shall present some HREM results concerning the accommodation of the precipitates with the surrounding matrix in the two cases, austenitic and martensitic matrix.

2. EXPERIMENTAL PROCEDURE

Single crystals of compositions *Cu* - 15.7 at% *Zn* - 16.3 at% *Al* (alloy 1, nominal Ms=263 K) and *Cu* - 12.9 at% *Zn* - 17.5 at% *Al* (alloy 2, nominal Ms=323 K) were grown by the Bridgman method. Several samples of both alloys were submitted to the suitable thermal treatments in order to generate the precipitates of γ phase [1-3,7]:

Alloy 1: 20' at 1120K, air cooling to 770K and quench into ice-water at 273K, followed by a heating to 670K for differents times t* (of the order of tenths of seconds) and subsequent quench into water at room temperature.

(1) Present address: Dept. de Física, Universitat de les Illes Balears, ctra. de Valldemossa km 7,5, 07071 Palma de Mallorca, Spain

Alloy 2: 20' at 1120K and quench to water at 330K (quench in parent phase), followed by a heating to 670K for 10s and quench to water at room temperature (quench to martensitic state).

The alloy 1 ($\beta + \gamma$ phases) was oriented by means of x-ray diffraction (Laue method) and several discs of 3 mm diameter and 0.2 mm thick were spark-cut on the $(100)_\beta$ and $(110)_\beta$ planes. The specimens of the alloy 2 (18R martensite + γ) were cut on a orientation which corresponds to the (111) plane of the parent β phase. The specimens were double-jet electropolished at room temperature until electron transparency. The HREM observations were performed in a Topcon EM002B unit operating at 200 kV. The HREM images were numerically simulated by means of the EMS software. In some cases, the images were digitalised and numerically processed by a selected filtering of the power spectrum of the image.

3. RESULTS AND DISCUSSION

3.1 Precipitates embedded in an austenitic matrix.

The HREM images of alloy 1 taken at atomic resolution reveal a perfect coherency between the β matrix and the γ precipitates, as it can be seen in figure 1. In this experimental micrograph, taken along the [100] zone axis, the continuity of the {010} and {011} planes in both phases is clearly visible. This is a consequence of the cube-cube type orientation relationships and the very small misfit between both structures (~0.7%). The coherency of the precipitates is lost when they reach sizes of about 50 nm, and misfit dislocations form in the interface. The characteristics of the misfit dislocations formed in semicoherent precipitates were reported in refs. [12-14]. Thus, we can conclude that the precipitates are well allocated inside the parent phase, i.e. the elastic and interfacial energies are relatively low. In the next section we will show that this is not the case when the precipitates are embedded in the martensitic phase.

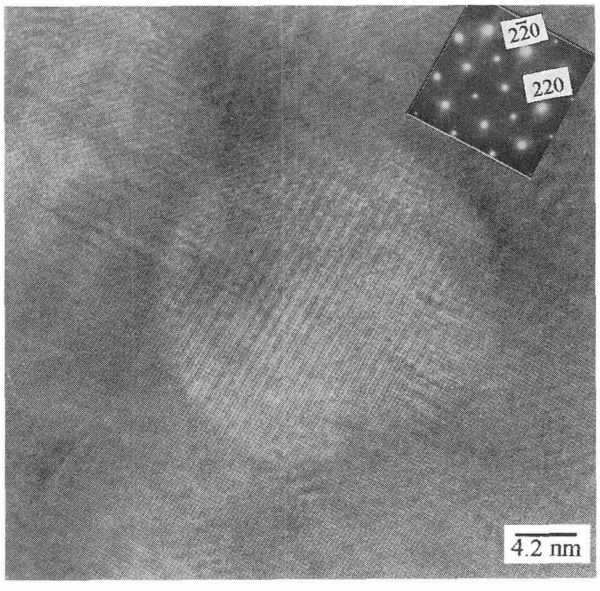

Figure 1. Atomic resolution HREM image of alloy 1 taken along the [001] zone axis, showing a coherent precipitate embedded in the β phase.

The figure 2 shows a HREM image taken wih an objective aperture that only selects the L21 superlattice spots of the [110]$_\beta$ zone axis. This fact enhances the image contrast and displays ordered domains and antiphase boundaries (APB). The micrographs taken in this manner show that the precipitates are located on the antiphase boundaries of the parent β phase. In this image the APB plane is inclined in relation to the zone axis, thus giving a blurred contrast. Comparing the experimental images with the simulations, it is possible to perform a reconstruction of the antiphase boundary at atomic level. The observed displacement of the atomic planes brought about by the APB can be obtained by two ways: *i)* shift of 1/2 L21 unit cell (one bcc basic cell) along <100>, giving rise to a next-nearest neighbours APB which swaps the *Al* and *Zn* atoms, not affecting the *Cu* sublattice (see fig. 3a), and, *ii)* shift of 1/4 L21 unit cell (one atomic layer) along the <110> direction, with the formation of a next-nearest neighbours APB changing both the *Cu* and *Zn/Al* sublattices (fig. 3b).

Small microdomains separated by antiphase-like boundaries are also present inside the precipitates, as can also be observed in figure 2. The presence of such microdomains in the γ precipitates was already reported by Lovey *et al* [15]. These microdomains were mostly observed in the specimens quenched from 770K. Their most remarquable effect is a slight shift of the diffraction spots leading to incommensurate diffraction patterns in relation to the β phase. After a subsequent flash heating the microdomains grow and, then, the number of boundaries decreases, which restablishes the commensurability of γ diffraction spots [15].

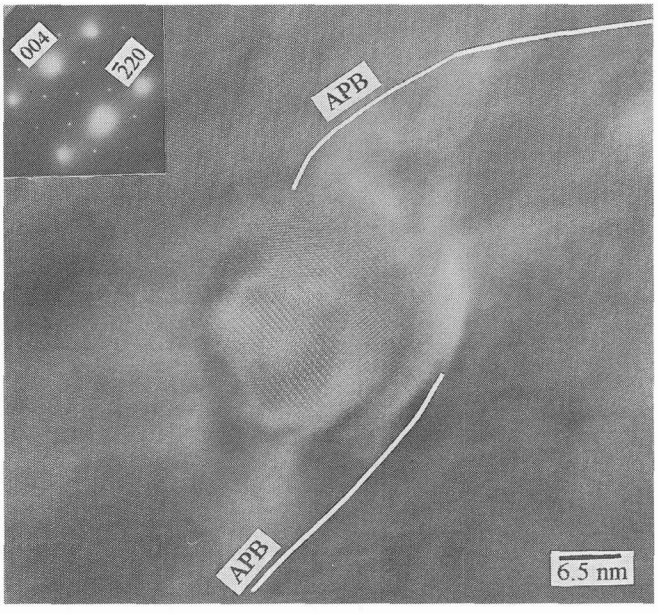

Figure 2. HREM image taken along the [110] zone axis, showing a precipitate located on an antiphase boundary of the matrix. Observe the presence of small microdomains inside the precipitates.

The analysis of the boundaries shows that the shift between two adjacent microdomains extends on one atomic layer along the <110> direction. The shear vector not being a translation vector of the lattice, the boundaries between the domains are not true antiphase boundaries but planar defects breaking the translational symmetry of the crystal (see figure 4). To get a true APB it is necessary a shift on the <110>

direction of one half of the projected unit cell, and it would be invisible in the experimental HREM images.

Note that the shear between two adjacent internal microdomains (one atomic layer on the <110> direction) coincides with one of the possibilities for the shear associated with the APB of the matrix. Then, the existence of internal microdomains could be thought as a consequence of the perfect coherency of the precipitates, which propagates the shear produced by the matrix APB into the precipitates. Nevertheless, a simple propagation of the APB inside the precipitates would form only two microdomains, whereas in the present investigations as well as in the work of ref [15], a large number of microdomains can be seen inside a single precipitate. Thus, the existence of these internal microdomains

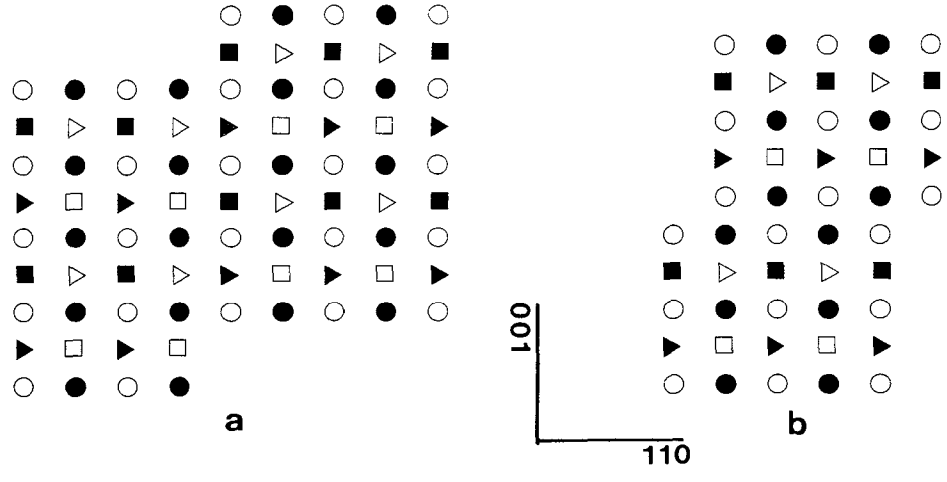

Figure 3. Atomic representation of the shift produced by the matrix APB (projected on the (110) plane), according to the experimental HREM images.
a) shift along <100> b) shift along <110>
O: Cu ▷: Zn □: Al
Open and full symbols represent atoms at different heights.

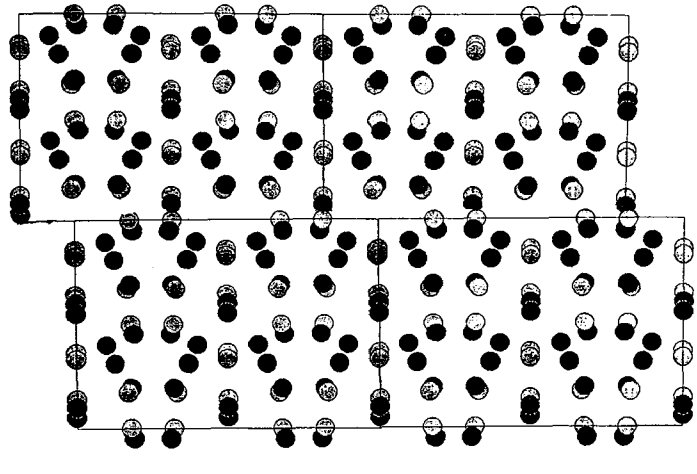

Figure 4. Atomic representation of the shift existing between two internal microdomains (in γ phase, projected on the (110) plane). We have considered the crystal structure of γ-brass [18].
Θ: Cu atoms ●: Zn atoms

seems to be an intrinsic feature of the γ-phase precipitates, and their relation with the matrix APB is, if any, secondary. In fact, inversion antiphase domains with <110> shears have indeed been observed and studied in the single phase γ-brass [16].

3.2 Precipitates embedded in a martensitic matrix.

As commented above, the precipitates are relatively well allocated inside the parent phase. But when this phase undergoes the martensitic transformation, due to the intrinsic deformation coming with the process, the accommodation between the martensite and the precipitates becomes difficult and this fact limits the growth of the martensite plates. The three sets of $\{100\}_\beta$ planes, i.e. (100), (010), (001), change their interplanar distance in a different way. One of them shortens by about 10%, another expands about 10% and the third practically does not change [17]. Conventional TEM observations showed that, when the precipitates are small, the martensite plates can still completely absorb the precipitates found during their growth, in such a way that a given precipitate is completely embbeded in a single martensite plate. Nevertheless, when the precipitates are bigger than ~0.5μm, the intrinsic shape change existing between the parent phase an a single variant of martensite becomes too large to be accommodated and, in turn, complex arrays of small selfaccommodating plates are formed around the precipitates, in order to reduce the global deformation [9].

In the present work, we focuss our attention to the first case (small precipitates), when the martensite plates can overcome the precipitates. In some cases, the precipitates are embedded in a main martensite plate and additional microplates of a second variant (belonging to the same selfaccomodating group) form around them. Looking at a nano-scale we have found this situation to occur as well. The figure 5a contains a HREM micrograph of alloy 2, showing a precipitate apparently embedded in a single martensite plate (at the CTEM scale). The image shows that a nanoplate, N, with a thickness of tens of atoms is formed between the main plate, M, (upper part of the image) and the precipitate, P, (in the bottom).

Another important feature can be observed in the enlarged framed region, figure 5b. The processed dot-type image (obtained by a selective filtering including all the intensity maxima of the power spectrum) evidences the presence of a dislocation-type defect. The Burgers circuit enclosing the defect reveals a Burgers vector lying in a direction which corresponds to the <100> direction of the parent phase.

Thus, even in the case of small precipitates, the accommodation between martensite and precipitate needs the formation of small selfaccommodating nanoplates at the interface with the precipitate, as well as dislocations. After the backtransformation to β phase, the dislocations formed in the martensite around the precipitates are inherited by the parent phase. A repetitive thermal cycling increases the number of dislocations in the matrix around the precipitates, forming dislocations arrays easily observable with the CTEM [9]. It has to be noted that the Burgers vector obtained in the present analysis of the HREM images, $\mathbf{b}=<100>_\beta$, coincides with the results obtained from the analysis of the CTEM images [9].

ACKNOWLEDGEMENTS

J.P. acknowledges the DGICyT (Spain) for the concession of a postdoctoral fellowship of MEC-MRT program.

REFERENCES

1. Rapacioli R., Chandrasekaran M.; "Precipitation in β Cu-Zn-Al" *Proc. Int. Conf. on Martensitic Transformations'79*, Cambridge Press MIT, 1979, p. 596
2. Rapacioli R., Chandrasekaran M., Lovey F.C.; "The influence of thermal treatments on martensitic transformation in Cu-Zn-Al alloys" *Proc. Int. Conf. on Solid-Solid Phase Transformations*; Carnegie Mellon Univ., 1981, p.739
3. Lovey F.C., Rapacioli R., Chandrasekaran M.; *Phys. Stat. Sol.* (a) **68** (1981) K105
4. Auguet C., Cesari E., Rapacioli R., Mañosa Ll.; *Scripta Metall.* **23** (1989) 579
5. Lovey F.C., Torra V., Isalgué A., Roqueta A., Sade M.; *Acta Metall. Mater.* **42** (1994) 453
6. Dutkiewicz J., Pons J., Cesari E.; *Mater. Sci. Eng.* **A158** (1992) 119
7. Pons J., Cesari E.; *Thermoch. Acta* **145** (1989) 237
8. Pons J., Cesari E., Roca M.; *Mater. Letters* **9** (1990) 542

9. Pons J., E. Cesari E.; *Acta Metall. Mater.* **41** (1993) 2547
10. Pons J., Sade M., Lovey F.C., Cesari E.; *Mat. Trans.,JIM* **34** (1993) 888
11. Isalgué A., Lovey F.C., Sade M.; *Scripta Metall. et Mater.* **28** (1993) 1183
12. Stephens D.E., Purdy G.R.; *Acta Metall.* **23** (1975) 1343
13. Lovey F.C., Cesari E.; *Mater. Sci. Eng.* **A129** (1990) 127
14. Chandrasekaran M., Pons J., Cesari E.; *Electron Microscopy, vol. 2, Proc. EUREM'92*, Granada, (1992) p.241
15. Lovey F.C., Van Tendeloo G., Van Landuyt J., Chandrasekaran M., Amelinckx S.; *Acta Metall.* **32** (1984) 879
16. Morton A.J.; *Phys. Stat. Sol (a)* **31** (1975) 661
17. Sade M., Hazarabedian A., Uribarri A., Lovey F.C.; "Effects of cycling through stress-induced martensitic transformations in Cu-Zn-Al alloys on dislocation structures and two-way memory",*Proc. Int. Conf. on Phase Transformations '87* (G.W. Lorimer, ed., The Institute of Metals, Cambridge), 1988 p. 279
18. Bradley A.J., Thewlis J.; *Proc. Roy. Soc.* **A112** (1926) 678

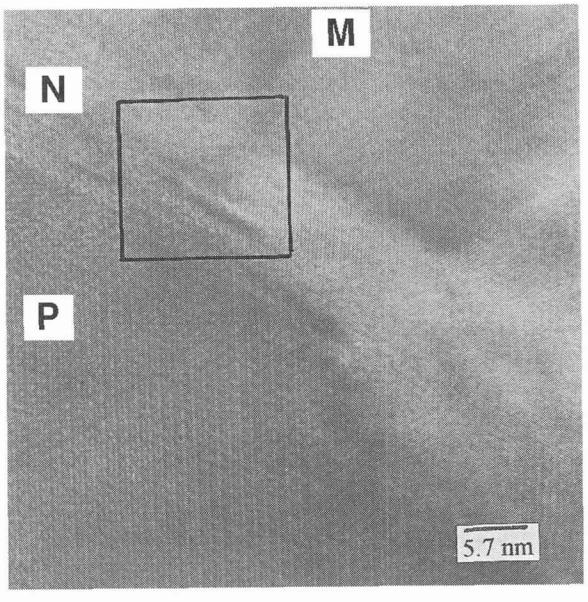

a

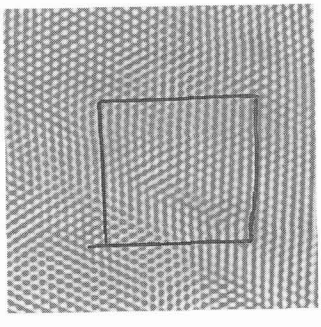

b

Figure 5. a) HREM image of alloy 2, showing a precipitate P embeded in a main martensite plate M, with a small nanoplate N at the interface.
b) enlarged processed image of the framed region of (a), showing a dislocation-type defect enclosed by a Burgers circuit.